ORIGINAL ARTICLE

Recognition of motion patterns using accelerometers for ataxic gait assessment

Ondřej Dostál[1] · Aleš Procházka[1,2,3] (ORCID) · Oldřich Vyšata[1] · Ondřej Ťupa[2] · Pavel Cejnar[2] · Martin Vališ[1]

Abstract

The recognition of motion patterns belongs to very important research areas related to neurology, rehabilitation, and robotics. It is based on modern sensor technologies and general mathematical methods, multidimensional signal processing, and machine learning. The present paper is devoted to the detection of features associated with accelerometric data acquired by 31 time-synchronized sensors located at different parts of the body. Experimental data sets were acquired from 25 individuals diagnosed as healthy controls and ataxic patients. The proposed method includes the application of the discrete Fourier transform for the estimation of the mean power in selected frequency bands and the use of these features for data segments classification. The study includes a comparison of results obtained from signals recorded at different positions. Evaluations are based on classification accuracy and cross-validation errors estimated by support vector machine, Bayesian, nearest neighbours (k-NN], and neural network (NN) methods. Results show that highest accuracies of 77.1%, 78.9%, 89.9%, 98.0%, and 98.5% were achieved by NN method for signals acquired from the sensors on the feet, legs, uplegs, shoulders, and head/spine, respectively, recorded in 201 signal segments. The entire study is based on observations in the clinical environment and suggests the importance of augmented reality to decisions and diagnosis in neurology.

✉ Aleš Procházka
Ales.Prochazka@vscht.cz

Ondřej Dostál
ondrej.dostal@fnhk.cz

Oldřich Vyšata
oldrich.vysata@fnhk.cz

Ondřej Ťupa
Ondrej.Tupa@vscht.cz

Pavel Cejnar
Pavel.Cejnar@vscht.cz

Martin Vališ
martin.valis@fnhk.cz

[1] Faculty of Medicine in Hradec Králové, Department of Neurology, Charles University in Prague, 500 05 Hradec Králové, Czech Republic

[2] Department of Computing and Control Engineering, University of Chemistry and Technology in Prague, 166 28 Prague 6, Czech Republic

[3] Czech Institute of Informatics, Robotics and Cybernetics, Czech Technical University in Prague, 160 00 Prague 6, Czech Republic

1 Introduction

Motion analysis has a wide range of applications in neurology, rehabilitation, and physical therapy, allowing the detection of motion disorders [7, 27] and monitoring of different neurological symptoms. This multidisciplinary area combines the knowledge and use of different micro-electromechanical sensor units (MEMS), video, depth and thermal camera systems [38, 39, 42], and wireless communication links. The development of automatic information systems in this area is a way how to contribute to the more efficient health care as well.

Computational intelligence methods process the data recorded by sensors located inside wearable devices, such as mobile phones [12, 18, 26] and tablets or more sophisticated systems including perception neuron [28, 35] and robotic devices. Specific sensors are often applied for gait analysis [1, 15, 47, 49, 53], gesture recognition [52], motion symmetry study [41], breathing [40], or for monitoring human activities [16, 17, 50]. The results of the

associated mathematical processing of the observed signals are then used for the early detection and classification of possible neurological disorders [46], monitoring the quality of the rehabilitation process, or for simulation-based training in surgery.

Motion sensors provide time-synchronized multichannel signals and multidimensional records that must be analysed by appropriate signal processing methods and specific intelligent data processing tools. While spatial domain features based on observations by video cameras are often used, frequency domain features can be very efficient as well. To avoid problems related the selection of the most significant features, the deep learning methods [2, 10, 45, 51] are used for more effective decision making in some cases as well. This complex approach [4, 21] to construction of classification models can be very efficient, but it needs sophisticated software and powerful computational tools.

The present paper is devoted to the analysis of motion feature [11, 22, 33] related to ataxia [13] as a neurological symptom characterized by the loss of balance and disrupted coordination while walking [7, 48]. Clinical scales used for diagnosing and quantification of ataxia (e.g. SARA) are not suitable for continuous monitoring in the natural environment of patients. In this situation, wearable sensors [19] can be very useful for balance assessment even though there are still many problems before their introduction to clinical practice. These problems include the selection of (1) the most suitable sensor positions, (2) the most determining features, and (3) the most reliable classification methods.

There exist different instrumented methods for objectification of ataxic disorders including infrared 3D cameras, pressure sensitive walkways [44], or electrooculography tests [32]. The increasing acceptance of gait analysis techniques and associated statistical analysis are enable to quantify subtle gait characteristics that are unmeasurable by current clinical methods to evaluate different gait scores and to differentiate between ataxic patients and healthy controls [7]. Despite of favourable results, no automated classification methods are commonly applied in the clinical practice.

Extracted parameters used for imbalance detection during the gait or stance represent spatio-temporal properties like the range of motions, step length, step time, stride time and speed, double support time, base width, and the anthropometric measures [9, 23]. A small number of studies bring promising results when extracting more complex features based on frequency measures [8, 29] and entropy [34, 37]. Specific studies are often devoted to the correlation of different biomedical and neurological signals [31], their interaction, and reactions to external stimuli.

The most common sensor placement is lower back and lower limb, while the locations on the upper body are relatively uncommon [19]. To analyse this problem, the full-body motion capture device (perception neuron [28]) was used to simultaneously record accelerometric data [3] at different sensor positions during the gait. Our set of individuals consists of healthy controls and ataxic patients suffering from multiple sclerosis (MS) as an autoinflammatory neurodegenerative disease.

The proposed method for the selection of features includes the use of functional transforms [25] to evaluate the components of the power at specific frequency ranges [24]. The extracted features are then used for the classification of the individual records and for evaluation of the classification accuracy for data acquired from different parts of the body.

2 Methods

2.1 Data acquisition

Figure 1 presents the principle of simultaneous data acquisition by the perception neuron system [5, 28] that uses 31 sensor units located at different parts of the body. This system enables both the data collection for the spatial location of the individual body joints and the recording of detailed signals acquired by individual sensors with a given sampling frequency. The notation for selected body positions used in the present study is presented in Table 1.

The individuals in Table 1 form two separate classes:

1. Normal: 13 individuals (95 time windows 20-s long),
2. Ataxic: 12 individuals (106 time windows 20-s long).

The diagnosis of these individuals was evaluated by two experienced neurologists according to their behaviour during the gait. The simultaneous recording of accelerometric data was performed by the perception neuron after its initial calibration. The sampling frequency was $f_s = 60$ Hz (sampling time period $T_s = 0.017$ s). Each time frame included accelerometric data in three directions for specific body positions. Their modulus was then used for the data analysis.

2.2 Data processing methods

The pattern matrix was formed by the column vectors of the features associated with each signal segment recorded at a specific body position. The distribution of power components was studied for each joint and signal segment separately, using the discrete Fourier transform and frequency windows 0.5 Hz long. A sample of the resulting plots for the left/right shoulder for all windows belonging
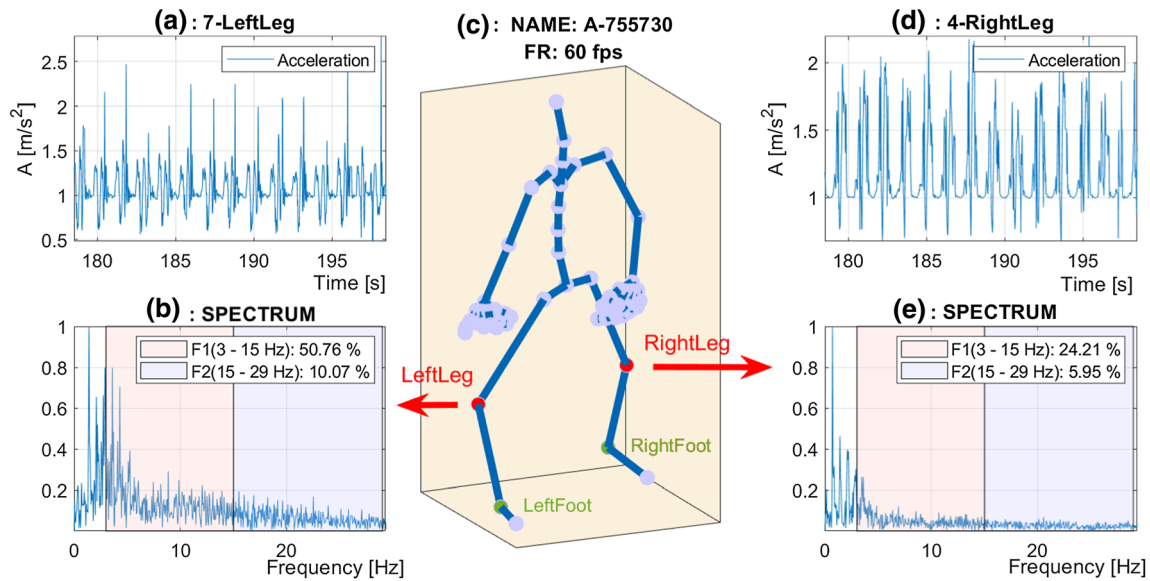
Fig. 1 Principle of the use of the axis neuron system for accelerometric data acquisition at a selected body position of an individual with ataxia presenting **a** data recorded from the left leg during a time window of 20 s; **b** its spectral components; **c** positions of the sensors; and **d**, **e** similar results for the right leg and spectral windows for the evaluation of the relative power and estimation of the data features

to a selected individual is presented in Fig. 2. Differences depend upon location of sensors and the diagnosis of a selected individual.

To reduce the number of features, two frequency ranges were selected to analyse the high-frequency components of the accelerometric data. Each of the selected spectral features of a signal segment N samples long was evaluated, using the discrete Fourier transform, in terms of the relative power in a specified frequency band $\langle f_{c1}, f_{c2} \rangle$, as follows:

$$PV = \frac{\sum_{k \in \Phi} |Y(k)|^2}{\sum_{k=0}^{M/2} |Y(k)|^2}, \quad Y(k) = \sum_{n=0}^{M-1} y(n)\, e^{-j k n \frac{2\pi}{M}} \quad (1)$$

where Φ is the set of indices for which the frequency values $f_k = \frac{k}{N} f_s \in \langle f_{c1}, f_{c2} \rangle$. In the given case, we studied accelerometric spectral features in $R = 2$ frequency bands, $\langle 3, 15 \rangle$ Hz and $\langle 15, 30 \rangle$ Hz.

The classification of Q pattern vector values and associated target values into two classes was performed by the methods of a support vector machine, Bayesian analysis, nearest neighbours, and neural networks. Special attention was given to the two-layer neural network as a classification model with R inputs, $S1$ neurons in the first layer, and $S2$ neurons in the second layer, as presented in Fig. 3.

The pattern matrix $\mathbf{P}_{R,Q}$ was formed by Q columns with each of them standing for a pattern vector associated with the individual accelerometric time window. The outputs of the individual layers formed the values

$$\begin{aligned} \mathbf{A1}_{S1,Q} &= F1(\mathbf{W1}_{S1,R}\, \mathbf{P}_{R,Q}, \mathbf{b1}_{S1,1}) \\ \mathbf{A2}_{S2,Q} &= F2(\mathbf{W2}_{S2,S1}\, \mathbf{A1}_{S1,Q}, \mathbf{b2}_{S2,1}) \end{aligned} \quad (2)$$

The network coefficients included the elements of the matrices $\mathbf{W1}_{S1,R}$, $\mathbf{W2}_{S2,S1}$ and vectors $\mathbf{b1}_{S1,1}$, $\mathbf{b2}_{S2,1}$. The matrix of target values $\mathbf{T}_{S2,Q}$ with $S2 = 2$ rows was defined by the corresponding classes specified by a neurologist.

The proposed model used the sigmoidal transfer function $F1$ in the first layer and the probabilistic softmax transfer function $F2$ in the second layer. The values of the output layer, based on the Bayes theorem [42], used the function

$$F2(.) = \frac{\exp(.)}{\text{sum}(\exp(.))} \quad (3)$$

which provides the probabilities of individuals' belonging to each class. The separate columns of the output matrix present the memberships in individual classes.

The performance of this neural network for its given target and evaluated outputs, $\mathbf{T}_{S2,Q}$ and $\mathbf{A2}_{S2,Q}$, respectively, was estimated by the cross-entropy error [30] and the calculation of the aggregate cross-entropy performance

$$P = \frac{1}{M} \sum_{i=1}^{S2} \sum_{j=1}^{Q} CE(i,j) \quad (4)$$

in each learning epoch with $M = S2 \times Q$ standing for the total number of output values and

$$\mathbf{CE}_{S2,Q} = -\mathbf{T}_{S2,Q}. * \log(\mathbf{A2}_{S2,Q}) \quad (5)$$

representing the cross-entropy for each pair of target–output elements. During the optimization process, the coefficients of the model were selected so as to minimize the cross-entropy values.

Table 1 Number of segments (S) belonging to class 1 (normal) and class 2 (ataxic) of separate individuals and positions used for extraction of accelerometric data features

Summary of individuals

Class 1: normal			Class 2: ataxic		
No.	Individual	S	No.	Individual	S
1	N-10	9	14	A-09	22
2	N-14	5	15	A-13	2
3	N-15	7	16	A-20	7
4	N-16	2	17	A-23	2
5	N-17	7	18	A-29	5
6	N-18	7	19	A-30	3
7	N-19	6	20	A-31	4
8	N-22	6	21	A-68	8
9	N-24	7	22	A-71	14
10	N-28	8	23	A-73	11
11	N-53	1	24	A-75	12
12	N-74	1	25	A-76	16
13	N-92	7			
Sum of segments		95	Sum of segments		106

Sensor location

Position	Name	Position	Name
2	RightUpLeg	6	LeftUpLeg
3	RightUp	7	LeftLeg
4	RightFoot	8	LeftFoot
17	RightShoulder	45	LeftShoulder
10	Spine	15	Head

NEURAL NETWORK FOR PATTERN RECOGNITION

Fig. 3 A two-layer neural network with sigmoidal and softmax transfer functions to recognize features of individual signal segments of accelerometric data acquired at specific body locations

3 Results

The proposed method was applied to the analysis of accelerometric data recorded at different body positions in 201 windows, each window being 20-s long (1200 samples), associated with two classes (normal and ataxic). After the initial detailed spectral analysis (presented for selected positions in Fig. 2), two frequency ranges for estimating the pattern values were chosen: $\langle 3, 15 \rangle$ Hz and $\langle 15, 30 \rangle$ Hz. Evaluations were done in the MATLAB 2019b environment.

Frequency domain signal processing is supported by [14, 36], confirming that sudden tilts during the gait cause three types of involuntary muscle responses. A segmental stretch reflex $M1$ occurs with a short latency, less than 50 ms, followed by the 'long loop' reflex $M2$ with its latency of 60–80 ms, and corrective muscle contractions, $M3$, at 100 ms. Patients with affected cerebellum or spinocerebellar pathways have delayed $M2$ or $M3$ reflexes. Moreover, such patients have a stronger and longer $M3$ antagonist response, which leads to correction overshooting. This is the most likely explanation for the higher power in the 3–15 Hz frequency range [33]. Inaccurate limb movements and dysfunctional corrective reflexes lead to increased body sway.

The comparison of the classification of the associated frequency features for the left and the right foot and for the left and the right shoulder for a selected individual (A09) is presented in Fig. 4. The selected individual belongs to the ataxic class, and the results show how symmetric parts of the body can be distinguished in case they behave differently.

Table 2 compares the average power features for 25 individuals and four positions on the left and right parts of the body: Left/RightFoot, Left/RightLeg, Left/RightUpLeg, and Left/RightShoulder. The results confirm that in
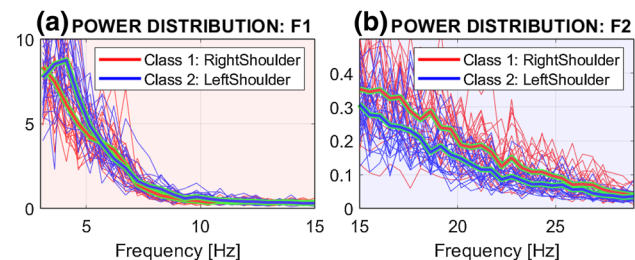

Fig. 2 The evolution of spectral components of a selected individual (A09) evaluated in a time window 20-s long estimated as the relative power in the frequency range **a** 3–15 Hz and **b** 15–30 Hz, respectively, for the left/right shoulder

The complete optimization process was performed for the training (70%), validation (15%), and test (15%) sets of signal segments. The qualities of the final models were then compared by their classification accuracy and the cross-validation errors.
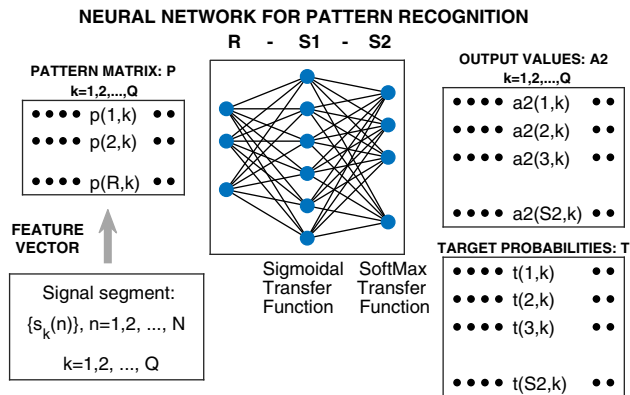
most cases, the average feature values for corresponding positions are lower for individuals from class 1 (normal) than for those from class 2 (ataxic). This fact can be explained by the body sway of ataxic patients and their efforts to compensate for instability.

Table 3 compares the average power features of 25 individuals and positions located on the head (15) and the spine (10). Again, the results confirm that in most cases, the average values of features for corresponding positions are lower for individuals from class 1 (normal) in comparison with those from class 2 (ataxic).

Figure 5 compares the distribution of the global mean of the power of a signal segment for 25 different individuals forming class 1 (normal) and class 2 (ataxic), using the mean power acquired by accelerometers located on the (a) left and right leg, (b) left and right upleg, (c) left and right shoulder, and (d) head and spine, using 20-s long time windows. The distribution of cluster centres with standard deviations for individual sensors located at different positions is presented in Fig. 6. The numerical comparison of clusters was performed by the criterion

$$C(k) = \frac{\text{dist}([M_x(j), M_y(j)], [M_x(k), M_y(k)])}{\text{mean}([S_x(j), S_y(j)]) + \text{mean}([S_x(k), S_y(k)])} \quad (6)$$

where $[M_x(i), M_y(i)]$ and $[S_x(i), S_y(i)]$ stand for cluster centres and standard deviations of cluster pairs for $i = j$ and $i = k$. This value is the highest for the shoulder position (3.0) and the lowest for the foot position (0.7).

Figure 7 compares selected classification results, and it presents the distribution of frequency features for the left foot, for the left upleg, and for the left shoulder, using data acquired from 25 individuals belonging to class 1 (normal) and class 2 (ataxic) using the neural network classification method. The clusters of values belonging to class 1 are more compact than those belonging to class 2, which have

Table 2 Comparison of average power features for 25 individuals and four positions on the left and right parts of the body: Left/RightFoot (8/4), Left/RightLeg (7/3), Left/RightUpLeg (6/2), and Left/RightShoulder (45/17)

Class	Ind.	Foot		Leg		UpLeg		Shoulder	
		F1	F2	F1	F2	F1	F2	F1	F2
Normal	1	30.8	9.7	37.8	11.8	44.9	5.6	22.4	0.6
	2	29.5	8.5	49.8	15.4	48.6	8.0	31.3	1.2
	3	34.2	8.7	47.1	8.3	38.1	7.2	27.7	1.2
	4	27.9	13.6	42.4	15.0	42.6	6.0	20.7	1.3
	5	28.4	7.5	34.8	9.4	42.1	4.5	38.0	0.9
	6	29.6	9.6	48.6	6.4	39.8	4.1	32.5	0.6
	7	27.3	11.4	47.0	13.3	37.2	11.6	32.8	1.8
	8	30.2	9.6	41.4	20.6	46.5	11.4	29.0	3.3
	9	26.9	10.4	47.1	15.5	42.0	10.5	17.1	5.7
	10	26.1	6.7	54.9	10.5	42.7	4.7	32.0	0.6
	11	23.2	6.1	53.7	13.3	46.3	6.6	26.6	0.6
	12	20.5	5.5	26.0	7.1	50.6	7.6	22.2	0.9
	13	25.3	6.9	35.2	14.8	46.9	6.7	20.9	0.6
	Mean	27.7	8.8	43.5	12.4	43.7	7.3	27.2	1.5
	SD	3.5	2.3	8.3	4.0	4.0	2.5	6.1	1.5
Ataxic	14	37.1	11.6	68.3	6.5	65.0	4.8	53.9	4.0
	15	25.3	10.1	43.0	9.1	52.1	6.3	41.4	1.5
	16	31.6	10.8	55.6	19.2	54.4	13.0	57.7	2.4
	17	37.5	14.2	48.5	15.1	57.9	13.1	49.2	1.4
	18	32.1	8.3	51.7	16.4	46.1	5.9	54.6	0.9
	19	45.6	13.3	51.0	11.4	60.8	6.2	70.4	3.2
	20	26.3	9.3	60.4	17.5	49.2	8.9	50.2	1.4
	21	40.9	11.8	56.4	10.9	61.8	9.1	63.4	0.8
	22	19.0	7.1	50.7	9.9	53.1	10.9	78.6	1.6
	23	34.0	6.3	56.1	5.8	54.4	5.6	45.0	1.1
	24	29.6	6.9	52.5	9.2	62.4	5.0	49.2	1.1
	25	38.0	13.3	42.2	9.4	56.2	11.5	64.8	1.6
	Mean	33.1	10.2	53.0	11.7	56.1	8.4	56.5	1.7
	SD	7.4	2.7	7.2	4.3	5.7	3.1	10.9	1.0

a larger standard deviation. Moreover, the discriminative abilities are higher for sensors located in the upper half of the body, confirming the results of other studies [15, 20].

Table 4 compares the classification accuracy by the support vector machine (SVM), decision tree (DT), 3-nearest neighbour (3-NN), and neural network (NN) methods for 25 individuals of class 1 (normal) and class 2 (ataxic) using power features acquired from accelerometers positioned on the left and right foot, leg, upleg, shoulder, and head/spine. Cross-validation errors are evaluated by the leave-one-out method in all cases.

The distribution of frequency features for both classes (1: healthy controls, 2: ataxic patients) and their

(a) CLASSIFICATION / ACC:70.5, CV:0.455

Class A: LeftFoot
Class B: RightFoot

F2 Power: 15-30 Hz [%]
F1 Power: 3-15 Hz [%]

(b) CLASSIFICATION / ACC:93.2, CV:0.182

Class A: LeftShoulder
Class B: RightShoulder

F2 Power: 15-30 Hz [%]
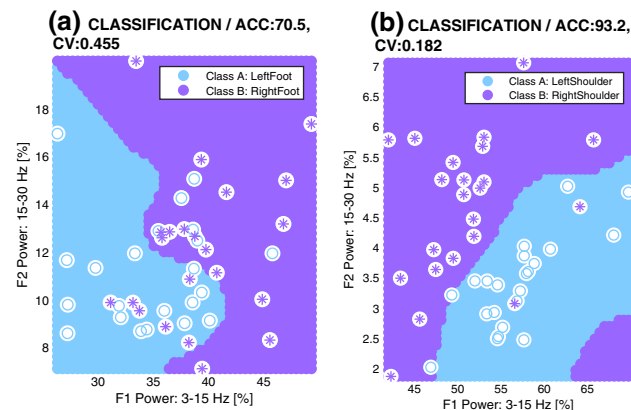F1 Power: 3-15 Hz [%]

Fig. 4 Classification of frequency features for **a** the left and right foot and **b** the left shoulder and right shoulder for a selected individual (A09) belonging to class 2 (ataxic)

Table 3 Comparison of average power features of 25 individuals and positions located on the head (15) and the spine (10) with their mean (MN) values

| Class	Ind.	Head F1	Head F2	Spine F1	Spine F2	Class	Ind.	Head F1	Head F2	Spine F1	Spine F2
Normal	1	29.5	5.5	33.3	2.6	Ataxic	14	55.1	7.4	52.7	3.2
	2	32.3	7.9	30.2	3.0		15	47.8	2.7	50.4	2.2
	3	29.3	11.6	35.9	3.4		16	55.6	13.6	48.6	4.8
	4	29.4	14.4	29.0	7.4		17	46.5	16.6	53.8	5.6
	5	34.1	4.5	41.2	1.4		18	53.8	4.3	55.5	2.1
	6	18.0	2.2	26.0	1.1		19	70.3	8.5	69.5	3.2
	7	36.3	16.8	40.6	5.0		20	56.2	7.0	52.8	3.5
	8	23.4	3.6	37.9	5.5		21	63.8	3.1	58.1	3.6
	9	22.1	14.2	21.6	9.4		22	69.4	6.2	64.3	2.3
	10	24.1	0.9	27.2	0.8		23	43.6	1.6	47.5	2.5
	11	18.5	3.3	23.5	1.3		24	40.7	2.3	48.4	1.6
	12	21.4	4.2	28.4	3.2		25	55.7	10.2	66.8	6.4
	13	25.4	5.7	25.3	2.8						
	Mean	26.4	7.3	30.8	3.6		Mean	54.9	7.0	55.7	3.4
	SD	5.9	5.2	6.5	2.6		SD	9.4	4.7	7.5	1.5
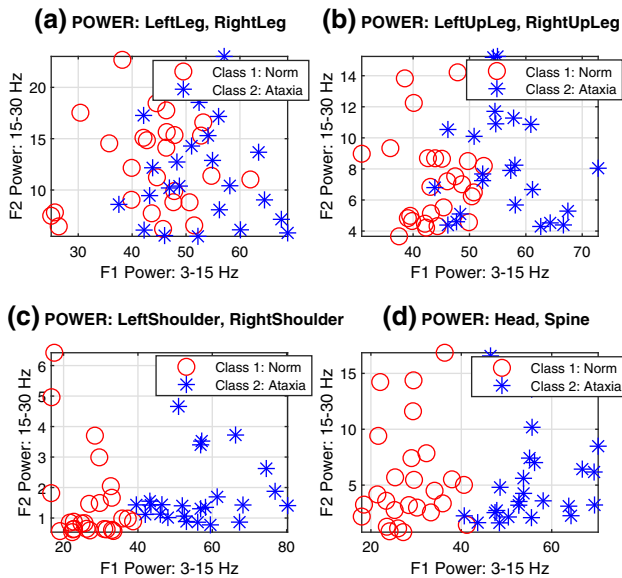
Fig. 5 Comparison of distributions of global mean power of signal segments for 25 different individuals forming class 1 (normal) and class 2 (ataxic) using mean power acquired by accelerometers located **a** left and right leg, **b** left and right upleg, **c** left and right shoulders, and **d** head and spine, using 20-s long time windows
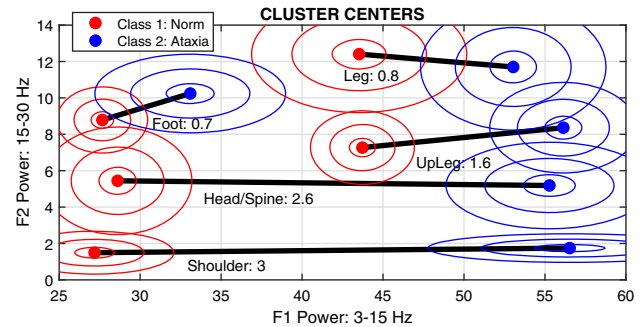

Fig. 6 The distribution of cluster centres for 25 different individuals forming class 1 (normal) and class 2 (ataxic) using mean power acquired by accelerometers located at different positions with 0.2, 0.5, and 0.8 multiples of standard deviations and criterion values for selected sensor positions

classification confirm the importance of their proper selection. It can be summarized that

1. cluster centres for class 1 (normal) are more compact than those of class 2 (ataxic): it can be explained by the different patterns of motion of patients with ataxia;
2. the relative mean power of features of patients with ataxia (in the frequency band F1 ⟨3, 15⟩ Hz) is higher, for the same reasons: this can be explained by the fast motions of patients with ataxia;
3. the classification accuracy is dependent on positions of sensors and the model used: sensors located on the shoulder, head, or spine can distinguish between classes 1 and 2 with an accuracy higher than 98%.

A better discrimination of ataxia with sensors placed on the upper body can be explained by comparison with the inverted pendulum. Ankle sensors capture less involuntary movements due to partial stabilization by the contact with the floor. Amplitude of body oscillations increases with the distance from the ground. Sensors placed on the head and shoulders are therefore more suitable for separation of normal and ataxic gait.

Results obtained correspond with those published recently [7, 29, 37]. Main advantages of accelerometric body-worn systems over other motion capture devices are in simultaneous monitoring of different body parts with
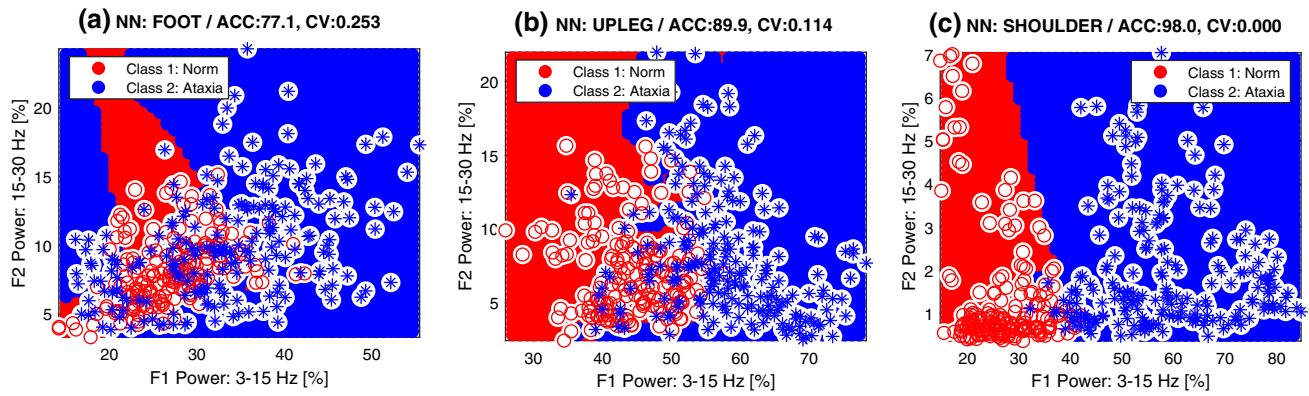
Fig. 7 Classification of frequency features for **a** the left foot, **b** the left upleg, and **c** the left shoulder, using data acquired from 25 individuals belonging to class 1 (normal) and class 2 (ataxic) using the neural network classification method and presenting the accuracy (AC) and cross-validation (CV) errors

Table 4 Accuracy (AC [%]), specificity (TNR [%]), sensitivity (TPR [%]), and cross-validation (CV) errors of the classification by the support vector machine (SVM), Bayesian, 3-nearest neighbour (3-NN), and neural network (NN) methods for power features acquired from accelerometers located on the left and right foot, leg, shoulder, and head/spine for 14 individuals of class 1 (normal) and class 2 (ataxic)

Position	Method	AC	TNR	TPR	CV
Left/right foot	SVM	76.2	88.9	66.4	0.251
	Bayes	67.9	80.5	55.2	0.326
	3-NN	75.3	86.8	83.9	0.289
	NN	78.1	87.4	69.8	0.246
Left/right leg	SVM	71.1	73.7	69.2	0.361
	Bayes	70.1	66.8	73.1	0.306
	3-NN	79.3	80.5	82.1	0.346
	NN	78.9	66.1	81.6	0.264
Left/right upleg	SVM	86.8	87.0	91.1	0.137
	Bayes	85.6	87.9	83.5	0.144
	3-NN	89.8	91.1	88.7	0.182
	NN	89.9	92.6	84.1	0.114
Left/right shoulder	SVM	97.3	96.8	97.6	0.027
	Bayes	97.0	97.4	96.7	0.030
	3-NN	97.0	98.4	95.8	0.047
	NN	97.6	97.9	97.2	0.012
Head/Spine	SVM	96.0	95.3	96.7	0.047
	Bayes	93.5	93.2	93.9	0.067
	3-NN	96.8	96.8	96.7	0.047
	NN	98.5	98.4	97.6	0.035

relatively high spatio-temporal resolution and extensive possibilities of feature extraction. Recording upper-body movements as a clinical biomarker during the gait is emerging as a powerful measure complementary to traditional gait analysis using stepping characteristics [6]. The proposed methodology is relatively simple and affordable for discriminating ataxic patients from controls. Different models using spatial domain features have in many cases much lower accuracy [32, 53] which in the early stage of the disease is between 70 and 80% [6, 43] only. These facts motivate further studies of accelerometers to diagnose ataxic disorders.

4 Conclusion

This paper presents selected methods of signal processing and machine learning to evaluate and classify accelerometric data acquired during the gait. Individuals selected by the clinical expert assessment include 12 ataxic patients and 13 healthy controls.

The goal of the study is to present the use of frequency domain features to classify individuals with neurological disorders and to study the discrimination abilities of sensors in dependence on their location on the body. Results show how different positions of sensors can affect the ability to perform the classification, its accuracy, and the cross-validation errors.

The study includes the application of selected classification methods to distinguish ataxic patients from healthy controls. The best results were achieved by the neural network method with the accuracy of 77.1 % for sensors located on the left/right foot that was increased to more than 98.0 % for sensors located in the upper part of the body (shoulders, head, spine).

It is expected that further studies will be devoted to the analysis of more extensive data sets of patients with different neurological problems during different kinds of activities and selected positions of sensors. Other features related to motion disorders (including spasticity, flaccidity, rigidity, tremor) will be studied as well. It is assumed that specific intelligent computational and classification

methods will contribute to the improvement of automatic diagnostic and monitoring tools for the daily medical practice.

Author contributions OD recorded all data and was responsible for their evaluation, AP was responsible for the mathematical and algorithmic tools, OV interpreted results from the neurological point of view, OT contributed to data preprocessing, PC contributed to evaluation of results, and MV was responsible for correct diagnostications of patients. All authors have read and approved the final manuscript.

Compliance with ethical standards

Conflict of interest The authors declare that there is no conflict of interests regarding the publication of this article.

Ethical approval All procedures involving human participants were in accordance with the ethical standards of the institutional research committee and with the 1964 Helsinki Declaration and its later amendments.

Informed consent Informed consent was obtained from all individual participants included in the study.

References

1. Allseits E, Kim K, Bennett C, Gailey R, Gaunaurd I, Agrawal V (2018) A novel method for estimating knee angle using two leg-mounted gyroscopes for continuous monitoring with mobile health devices. Sensors 18:2759:1–2759:17
2. Almaslukh B, Artoli A, Al-Muhtadi J (2018) A robust deep learning approach for position-independent smartphone-based human activity recognition. Sensors 18(11):3726
3. Alvarez D, Alvarez J, Gonzalez R, Lopez A (2015) Upper limb joint angle measurement in occupational health. Comput Methods Biomech Biomed Eng 19(2):1–12
4. Antoniades A, Spyrou L, Martin-Lopez D, Valentin A, Alarcon G, Sanei S, Took C (2017) Detection of interictal discharges with convolutional neural networks using discrete ordered multi-channel intracranial EEG. IEEE Trans Neural Syst Rehabil Eng 25(12):2285–2294
5. Baumann T, Hao T, He Y, Shoda R (2017) Perception neuron unity handbook, 027th edn. Noitom Technology Co. Ltd, St Miami
6. Buckley C, Alcock L, McArdle R, Rehman R, Din S, Mazzà C, Yarnall AJ, Rochester L (2019) The role of movement analysis in diagnosing and monitoring neurodegenerative conditions: insights from gait and postural control. MDPI Br Sci 19:34:1–34:21
7. Buckley E, Mazza C, McNeill A (2018) A systematic review of the gait characteristics associated with Cerebellar Ataxia. Gait Posture 60:154–163
8. Caliandro P, Conte C, Iacovelli C, Tatarelli A, Castiglia S, Reale G, Serrao M (2019) Exploring risk of falls and dynamic unbalance in cerebellar ataxia by inertial sensor assessment. Sensors 19(24):5571:1–5571:9
9. Caramia C, Torricelli D, Schmid M, Munoz-Gonzalez A, Gonzalez-Vargas J, Grandas F, Pons J (2018) IMU-based classification of Parkinson's disease from gait: a sensitivity analysis on sensor location and feature selection. IEEE J Biomed Health Inf 22(6):1765–1774
10. Chambon S, Galtier M, Arnal P, Wainrib G, Gramfort A (2018) A deep learning architecture for temporal sleep stage classification using multivariate and multimodal time series. IEEE Trans Neural Syst Rehabil Eng 26(4):758–769
11. Chen P, Kuang Y, Li J (2016) Human motion capture algorithm based on inertial sensors. J Sens 2016:4343,797:1–4343,797:15
12. Chen Y, Shen C (2017) Performance analysis of smartphone-sensor behavior for human activity recognition. IEEE Access 5:3095–3110
13. D'Ambrosio A, Pagani E, Riccitelli G, Colombo B, Rodegher M, Falini A, Comi G, Filippi M, Rocca M (2017) Cerebellar contribution to motor and cognitive performance in multiple sclerosis: an MRI sub-regional volumetric analysis. Mult Scler 23(9):1194–1203
14. Diener H, Dichgans J, Bacher M, Guschlbauer B (1984) Characteristic alterations of long-loop "reflexes" in patients with Friedreich's disease and late atrophy of the cerebellar anterior lobe. J Neurol Neurosurg Psych 47(7):679–685
15. Din S, Hickey A, Hurwitz N, Mathers J, Rochester L, Godfrey A (2016) Measuring gait with an accelerometer-based wearable: influence of device location, testing protocol and age. Physiol Meas 37:1785–1797
16. Ebara T, Azuma R, Shoji N, Matsukawa T, Yamada Y, Akiyama T, Kurihara T, Yamada S (2017) Reliability of smartphone-based gait measurements for quantification of physical activity/inactivity levels. J Occup Health 59(6):506–512
17. Ellis K, Kerr J, Godbole S, Lanckriet G, Wing D, Marshall S (2014) A random forest classifier for the prediction of energy expenditure and type of physical activity from wrist and hip accelerometers. Physiol Meas 35(11):2191–2203
18. Fuentes D, Gonzalez-Abril L, Angulo C, Orteg J (2012) Online motion recognition using an accelerometer in a mobile device. Expert Syst Appl 39(3):2461–2465
19. Ghislieri M, Gastaldi L, Pastorelli S, Tadano S, Agostini V (2019) Wearable inertial sensors to assess standing balance: a systematic review. Sensors 19:4075:1–4075:25
20. Goldsztein G (2017) Modeling walking with an inverted pendulum not constrained to the sagittal plane. Numerical simulations and asymptotic expansions. Appl Math 8:57–76
21. Goodfellow I, Bengio Y, Courville A (2016) Deep learning. MIT Press, Cambridge
22. Grimaldi G, Manto M (2010) Neurological tremor: sensors, signal processing and emerging applications. MDPI Sens 10:1399–1422
23. Hasegawa N, Shah V, Carlson-Kuhta P, Nutt J, Horak F, Mancini M (2019) How to select balance measures sensitive to Parkinsons disease from body worn inertial sensors separating the trees from the forest. Sensors 19:3320:1–3320:18
24. Hong F, You S, Wei M, Zhang Y, Guo Z (2016) OMGRA: motion gesture recognition via accelerometer. MDPI Sens 16:530:1–531:25
25. Hošt'álková E, Vyšata O, Procházka A (2007) Multi-dimensional biomedical image de-noising using Haar transform. In: Proceedings of the 15th international conference on digital signal processing. IEEE, Cardiff, UK, pp 175–179

26. Ishikawa M, Yamada S, Yamamoto K, Aoyagi Y (2019) Gait analysis in a component timed-up-and-go test using a smartphone application. J Neurol Sci 398:45–49

27. Joukov V, Bonnet V, Karg M, Venture G, Kulic D (2018) Rhythmic extended Kalman filter for gait rehabilitation motion estimation and segmentation. IEEE Trans Neural Syst Rehabil Eng 26(2):407–418

28. Kim H, Hong N, Kim M, Yoon S, Yu H, Kong H, Kim S, Chai Y, Choi H, Choi J, Lee K, Kim S, Kim H (2019) Application of a perception neuron system in simulation-based surgical training. MDPI J Clin Med 8:124:1–124:14

29. Krishna R, Pathirana P, Horne M, Power L, Szmulewicz D (2019) Quantitative assessment of cerebellar ataxia, through automated limb functional tests. J Neuroeng Rehabil 16:31:1–31:15

30. Kusumoputro B, Lina B (2016) Infrared face recognition system using cross entropy error function based ensemble backpropagation neural networks. IJCTE 8:161–166

31. Li H, Trocan M (2018) Deep learning of smartphone sensor data for personal health assistance. Microelectron J 88:164–172

32. López A, Ferrero F, Postolache O (2019) An affordable method for evaluation of ataxic disorders based on electrooculography. MDPI Sens 19(17):3756:1–3756:16

33. Marsden JF (2018) Chapter 17—Cerebellar ataxia. In: Day BL, Lord SR (eds) Balance, gait, and falls, handbook of clinical neurology, vol 159. Elsevier, Amsterdam, pp 261–281

34. Nguyen N, Phan D, Pathirana P, Horne M, Power L, Szmulewicz D (2018) Quantification of axial abnormality due to cerebellar ataxia with inertial measurements. Sensors 18(9):2791:1–2791:15

35. Ohashi H, Al-Naser M, Ahmed S, Nakamura K, Sato T, Dengel A (2018) Attributes importance for zero-shot pose-classification based on wearable sensors. MDPI Sens 18(8):2485:1–2485:17

36. Petersen N, Christensen L, Morita H, Sinkjaer T, Nielsen J (1998) Evidence that a transcortical pathway contributes to stretch reflexes in the tibialis anterior muscle in man. J Physiol 512(1):267–276

37. Phan D, Nhan N, Pathirana P, Horne M, Power L, Szmulewicz D (2019) Quantitative assessment of ataxic gait using inertial sensing at different walking speeds. In: IEEE engineering in medicine and biology, EMBC, pp 4600–4603

38. Procházka A, Charvátová H, Vaseghi S, Vyšata O (2018) Machine learning in rehabilitation assessment for thermal and heart rate data processing. IEEE Trans Neural Syst Rehabil Eng 26(6):1209–1214

39. Procházka A, Charvátová H, Vyšata O, Kopal J, Chambers J (2017) Breathing analysis using thermal and depth imaging camera video records. MDPI Sens 17:1408:1–1408:10

40. Procházka A, Schatz M, Centonze F, Kuchyňka J, Vyšata O, Vališ M (2016) Extraction of breathing features using MS Kinect for sleep stage detection. Signal Image Video Process 10(7):1278–1286

41. Procházka A, Vyšata O, Charvátová H, Vališ M (2019) Motion symmetry evaluation using accelerometers and energy distribution. Symmetry 11:871:1–871:13

42. Procházka A, Vyšata O, Vališ M, Tupa O, Schatz M, Mařík V (2015) Bayesian classification and analysis of gait disorders using image and depth sensors of Microsoft Kinect. Digit Signal Process 47(12):169–177

43. Rizzo G, Copetti M, Arcuti S, Martino D, Fontana A, Logroscino G (2016) Accuracy of clinical diagnosis of Parkinson disease: A systematic review and meta-analysis. Neurology 86(3):566–576

44. Roche B, Simon A, Guilmin-Crépon S, Boizeau B, Andriss B, Alberti C, Presedo A, Ilharreborde B, Husson I (2018) Test-retest reliability of an instrumented electronic walkway system (GAI-TRite) for the measurement of spatio-temporal gait parameters in young patients with Friedreich's ataxia. Gait Posture 66:45–50

45. Sadouk L, Gadi T (2019) Convolutional neural networks for human activity recognition in time and frequency-domain. Adv Intell Syst Comput 756:485–496

46. Sanei S, Chambers J (2007) EEG signal processing. Wiley, New York

47. Staab W, Hottowitz R, Sohns C, Sohns J, Gilbert F, Menke J, Niklas A, Lotz J (2014) Accelerometer and gyroscope based gait analysis using spectral analysis of patients with osteoarthritis of the knee. J Phys Ther Sci 26:997–1002

48. Stolze H (2002) Typical features of cerebellar ataxic gait. J Neurol Neurosurg Psych 73:310–312

49. Sun B, Wang Y, Banda J (2014) Gait characteristic analysis and identification based on the iphone accelerometer and gyrometer. Sensors 18:17037–17054

50. Voicu R, Dobre C, Bajenaru L, Ciobanu R (2019) Human physical activity recognition using smartphone sensors. MDPI Sens 19:458:1–4581:18

51. Wang J, Chen Y, Hao S, Peng X, Hu L (2019) Deep learning for sensor-based activity recognition: a survey. Pattern Recognit Lett 119:3–11

52. Xu R, Zhou S, Li W (2012) MEMS accelerometer based non-specific-user hand gesture recognition. IEEE Sens J 12:1166–1173

53. Zilani T, Al-Turjman F, Khan M, Zhao N, Yang X (2020) Monitoring movements of ataxia patient by using UWB technology. MDPI Sens 20:931:1–931:16

Publisher's Note Springer Nature remains neutral with regard to jurisdictional claims in published maps and institutional affiliations.